# Synthesis of bombesin-functionalized iron oxide nanoparticles and their specific uptake in prostate cancer cells

**Amanda L. Martin**,
Department of Chemistry, The University of Western Ontario, 1151 Richmond St., London, ON N6A 5B7, Canada

**Jennifer L. Hickey**,
Department of Chemistry, The University of Western Ontario, 1151 Richmond St., London, ON N6A 5B7, Canada

**Amber L. Ablack**,
Department of Oncology, The University of Western Ontario, 1151 Richmond St., London, ON N6A 5B7, Canada

**John D. Lewis**,
Department of Oncology, The University of Western Ontario, 1151 Richmond St., London, ON N6A 5B7, Canada, Department of Medical Biophysics, The University of Western Ontario, 1151 Richmond St., London, ON N6A 5B7, Canada

**Leonard G. Luyt**, and
Department of Chemistry, The University of Western Ontario, 1151 Richmond St., London, ON N6A 5B7, Canada, Department of Oncology, The University of Western Ontario, 1151 Richmond St., London, ON N6A 5B7, Canada, Department of Medical Imaging, The University of Western Ontario, 1151 Richmond St., London, ON N6A 5B7, Canada

**Elizabeth R. Gillies**
Department of Chemistry, The University of Western Ontario, 1151 Richmond St., London, ON N6A 5B7, Canada, Department of Chemical and Biochemical Engineering, The University of Western Ontario, 1151 Richmond St., London, ON N6A 5B7, Canada

## Abstract

The imaging of molecular markers associated with disease offers the possibility for earlier detection and improved treatment monitoring. Receptors for gastrin-releasing peptide are overexpressed on prostate cancer cells offering a promising imaging target, and analogs of bombesin, an amphibian tetradecapeptide have been previously demonstrated to target these receptors. Therefore, the pan-bombesin analog [$\beta$-Ala11, Phe13, Nle14]bombesin-(7–14) was conjugated through a linker to dye-functionalized superparamagnetic iron oxide nanoparticles for the development of a new potential magnetic resonance imaging probe. The peptide was conjugated via click chemistry, demonstrating a complementary alternative methodology to

conventional peptide-nanoparticle conjugation strategies. The peptide-functionalized nanoparticles were then demonstrated to be selectively taken up by PC-3 prostate cancer cells relative to unfunctionalized nanoparticles and this uptake was inhibited by the presence of free peptide, confirming the specificity of the interaction. This study suggests that these nanoparticles have the potential to serve as magnetic resonance imaging probes for the detection of prostate cancer.

## Keywords

Iron oxide; Nanoparticles; Bombesin; Prostate cancer; Magnetic resonance imaging; Nanomedicine

## Introduction

Molecular imaging, the non-invasive visualization of cellular function and molecular processes, is emerging as a highly promising tool for detecting disease and improving treatments (Ametamey et al. 2008; Cai and Chen 2008; Weissleder and Pittet 2008; Willmann et al. 2008). Many different imaging modalities including magnetic resonance imaging (MRI), optical imaging, single photon emission computed tomography (SPECT), positron emission tomography (PET), and ultrasound are available, each with accompanying advantages and disadvantages. MRI has the advantages of high spatial resolution and excellent delineation of anatomical structure and does not involve high energy radiation (Basilion et al. 2005). While the sensitivity of MRI is lower than modalities such as SPECT and PET, traditionally requiring contrast agent concentrations in the high micromolar to millimolar range (Caravan et al. 1999), superparamagnetic iron oxide nanoparticles (SPIO) have emerged as useful probes in cellular and molecular imaging due to their high sensitivity, allowing them to be used at lower doses than paramagnetic probes based on $Gd^{3+}$ (Jun et al. 2008; Laurent et al. 2008). In addition, polymer-coated nanoparticles provide ideal nanoscale scaffolds for the conjugation of multiple copies of targeting ligands, drugs, or contrast agents for other imaging modalities (Hosseinkhani and Hosseinkhani 2009). While optical imaging often suffers from a lack of penetration depth in vivo, it offers an ideal complement to MR in the initial screening of new probes (Weissleder and Pittet 2008).

Prostate cancer is the second most common form of cancer found in men in North America (American Cancer Society 2007). It is known to spread through metastasis and can progress without symptoms for many years, making diagnosis and treatment challenging. Currently, a common method for the detection of prostate cancer is a blood test known as the prostate specific antigen test. However, doubts have been raised about the accuracy and usefulness of this test (Nam et al. 2007). Another test is the digital rectal exam which measures the size and texture of the prostate gland manually (Chodak et al. 1989). Any irregularities found would be further examined using biopsy. While relatively effective, this is a highly invasive procedure, which only allows for 85% of the prostate to be examined. MRI is a promising and less invasive way to diagnose prostate cancer. For example, $T_2$ (Heijmink et al. 2007; Ikonen et al. 2001; Kirkham et al. 2006), and diffusion (Ikonen et al. 2001; Tanimoto et al. 2007) weighted sequences have been investigated. Other developments have involved the use of magnetic resonance spectroscopy (Huzjan et al. 2005; Zapotoczna et al. 2007) or dynamic

contrast enhanced MRI using $Gd^{3+}$ agents that access tumors due to their enhanced vascular permeability (Alonzi et al. 2007; Padhani et al. 2000). However, there are only a few recent examples of MRI contrast agents targeted specifically to prostate cancer cells. Antibodies (Serada et al. 2007) and aptamers (Wang et al. 2008) targeting the prostate-specific membrane antigen expressed on prostate cancer cells have been conjugated to SPIO, facilitating selective binding and uptake. Selective imaging of prostate cancer cells in vivo was also recently achieved by the conjugation of SPIO to peptides targeting hepsin, a prostate cancer biomarker (Kelly et al. 2008).

Gastrin-releasing peptide (GRP) and its receptors are clearly linked to cancer, with over-expression of the receptors found in many cancer types and especially prostate cancer (Patel et al. 2006; Sun et al. 2000). Radionuclide probes based on bombesin, an amphibian tetradecapeptide, have been reported to specifically target GRP overexpressing tumors (Hoffman et al. 2003; Van de Wiele et al. 2000). Four different receptor sub-types were discovered for the GRP family of peptides: GRP-R, neuromedin-B receptor (NMB-R), BRS-3, and BB4-R. A very potent ligand for all four bombesin receptor sub-types was previously reported, with a structure of [D-Tyr6, $\beta$-Ala11, Phe13, Nle14]bombesin-(6–14) (Mantey et al. 1997; Pradhan et al. 1998; Reubi et al. 2002).

Described here is the synthesis of an alkyne derivatized bombesin peptide and its conjugation to azide-functionalized SPIO, with the aim of developing for the first time, a bombesin-targeted MR probe for the selective imaging of prostate cancer cells. Prior to this work, there was only one previous report of bombesin-functionalized SPIO, but the agent was developed for targeting normal pancreatic cells in order to visualize pancreatic ductal adenocarcinoma in an inverse imaging strategy (Montet et al. 2006). Its uptake by prostate cancer cells was not investigated. In addition, in contrast to the previous report, the bombesin derivative used in this work contains unnatural amino acid substitutions aimed at enhancing its resistance to proteases, while the alkyne allows for a facile click reaction to be carried out without the use of protecting groups or activation steps to conjugate the peptide to the nanoparticles. A fluorescent rhodamine derivative was also conjugated to the nanoparticles to provide an optical probe to facilitate the in vitro evaluation described here. The selective uptake of these bombesin-functionalized nanoparticles relative to control nanoparticles in PC-3 prostate cancer cells is demonstrated in vitro.

## Experimental procedures

### General procedures and materials

All chemicals were purchased from commercial sources and used without further purification unless otherwise noted. Dialysis was performed using a 25 kDa molecular weight cut-off (MWCO) Spectra/Por regenerated cellulose membrane. Ultrafiltration was carried out using a 300 kDa MWCO membrane of polyethersulfone purchased from Amicon. Infrared spectra were obtained as KBr pellets. Transmission electron microscopy (TEM) was carried out using a carbon formvar grid and a Phillips CM10 microscope operating at 80 kV with a 40 μm aperture. Dynamic light scattering (DLS) was performed at a concentration of 1 mg of iron/mL in water using a Malvern Zetasizer Nano-S instrument. Analytical HPLC was performed using a Grace Vydac Protein/Peptide RP-C18 column 4.6

× 250 mm, 5 μm. Preparative HPLC was performed using a Grace Vydac Protein/Peptide RP-C18 column 22.0 × 250 mm, 10 μm. A gradient system was used consisting of: $CH_3CN$ + 0.1% of TFA (solvent A) and $H_2O$ + 0.1% of TFA (solvent B) and the absorbance was detected at wavelengths of 220 and 254 nm. The Electrospray Ionization mass spectrum was obtained using a Micromass Quatro Micro LCT mass spectrometer.

### Synthesis of peptide 1

Fully protected resin-bound peptides were synthesized via standard Fmoc solid phase peptide chemistry using both manual peptide synthesis methods and an APEX 396 automated peptide synthesizer. Fmoc protected rink amide MBHA resin (loading 0.47 meq/g) was utilized as the solid support. All *N*-Fmoc amino acids were employed, with propargylacetic acid used to install the alkyne functionality at the *N*-terminus of the peptide. Fmoc removal was achieved by treatment with 20% piperidine in DMF for 5 and 20 min with consecutive DMF and $CH_2Cl_2$ washes after each treatment. For each Fmoc amino acid coupling, the resin was treated twice with 3 eq. of Fmoc amino acids, 3 eq. of HBTU and 6 eq. of DIPEA in 2 mL of DMF for 30 min to 2 h. The resin was washed consecutively with DMF, $CH_2Cl_2$, and THF following each coupling. When coupling the propargylacetic acid, the resin was treated twice as above followed by a third coupling consisting of 5 eq. of alkyne, 5 eq. of HBTU, and 10 eq. of DIPEA in 5 mL of DMF for 16 h.

Once the linear sequence was complete, the peptide was deprotected and cleaved from the resin by treatment with TFA containing water (5% v/v), phenol (5% m/v) and triisopropylsilane (TIS) (2% v/v) as scavengers for 4 h. The resin was filtered and rinsed with a small amount of TFA. The resulting peptide was then precipitated from the TFA solution using tert-butyl methyl ether (TBME), and collected after centrifugation and decantation. The peptide was then rinsed with TBME and centrifugation and decantation was repeated. The resulting solid was redissolved in water and lyophilized to obtain the crude peptide. Purification was carried out by preparative HPLC (linear gradient of 20–80% solvent A in B) with the purity of the isolated white fluffy peptide **1** determined to be 98.7% by analytical HPLC. Yield: 23.5 mg (12%). MS (ESI): m/z calcd 1121.59, found 1121.35 $[M+H]^+$.

### Synthesis of peptide-functionalized nanoparticle 4

Nanoparticle **2** was prepared as previously reported (Martin et al. 2008; Molday and MacKenzie 1982; Pittet et al. 2006), having 1.0 μmol of azide/mg of iron and 0.1 μmol of rhodamine **3**/mg of iron. To a solution of these nanoparticles in water (1 mg of Fe in 1.0 mL of water, 1.0 μmol azide) was added peptide **1** (2.3 mg, 2.0 μmol, 2.0 equiv. per azide) dissolved in DMF (0.5 mL), followed by sodium ascorbate (2.0 mg, 10 μmol) and $CuSO_4$ (1.0 mg, 3.7 μmol). The reaction mixture was stirred overnight and was then dialyzed against 10 mM ethylenediaminetetraacetic acid (EDTA), followed by pure water to yield the functionalized nanoparticle **4**. The sample was then concentrated using ultrafiltration to an iron concentration of 0.5 mg/mL.

## Quantification of functionalization yield

The iron concentrations of solutions of nanoparticles **2** and **4** were determined by degradation of the nanoparticles with hydrochloric acid and hydrogen peroxide, followed by measurement of their absorbance at 344 nm and comparison against a calibration curve (Pittet et al. 2006). Solutions containing the same quantity of iron for each sample were lyophilized, then converted to KBr pellets using the same quantities of KBr. Infrared (IR) spectra were obtained from 500–4000 cm$^{-1}$, and the integrations of the peaks at 2,090 cm$^{-1}$ corresponding to the azide stretch were compared, providing an approximate reaction yield of 83%. The peak at 845 cm$^{-1}$ on the nanoparticle can also be used as an internal standard, as the peptide exhibits no absorbance in this range, providing an approximate reaction yield of 80%. Subjection of the nanoparticles to the reaction conditions in the absence of the alkyne did not lead to any reduction in the peak at 2,090 cm$^{-1}$.

## Cell uptake experiment

Human prostate cancer PC-3 cells (ATCC, Manassas, VA), cultured in F-12 media (Invitrogen, Carlsbad, CA), were transfected with a PCDNA3.1neo$^R$-GFP vector and stabilized under selection in media containing G418 (Invitrogen, Carlsbad, CA) to express GFP throughout the cytoplasm. Approximately 10,000 PC-3-GFP cells were plated in a 12-well tissue culture plate containing circular glass cover slips. After incubation overnight, 20 μg each of nanoparticle **2** (control) or nanoparticle **4** (experimental) was added to the culture media and incubated for 2 h at 37 °C. For the blocking experiment, a ten-fold excess of peptide **1** (15 μM final concentration) was added to the culture media and incubated at 37 °C for 30 min prior to the addition of 20 μg of nanoparticle **4**. Cells were then washed with media (3×), fixed with ice-cold 4% paraformaldehyde in PBS for 10 min, washed with PBS (3x), and mounted using Prolong Gold mounting medium containing DAPI (Invitrogen). The cells were photographed using a 63× immersion lens and a Hamamatsu EM-CCD camera under a Zeiss AxioImager Z1 microscope.

# Results and discussion

## Peptide synthesis

The peptide analog [D-Tyr6, $\beta$-Ala11, Phe13, Nle14]bombesin-(6–14) is a universal bombesin ligand, which has been shown to bind to all four GRP receptor sub-types with high affinity (Mantey et al. 1997; Pradhan et al. 1998; Van de Wiele et al. 2000). The GRP family of receptors are known to be over-expressed in a variety of human tumors, including prostate cancer, making the pan-bombesin peptide a potentially important targeting entity for both cancer diagnosis and treatment (Patel et al. 2006; Sun et al. 2000). To date, the only reported bombesin-functionalized iron oxide nanoparticles were synthesized by Montet et al. to target normal pancreatic cells via an inverse imaging strategy (Montet et al. 2006). They utilized an unmodified bombesin peptide composed entirely of natural $\alpha$-amino acids; however, the universal pan-bombesin ligand has an advantage over natural bombesin as it incorporates unnatural amino acids such as D-Tyr and a $\beta$-alanine spacer, both allowing for greater protease resistance.

Previously, the truncated bombesin-(7–14) sequence was proven to be sufficient for binding interactions with the GRP receptor (Broccardo et al. 1975; Girard et al. 1984). In fact, there have been various radiolabeled bombesin conjugates containing extensive modifications to the *N*-terminus, which still retain high affinity for the desired receptors (Baidoo et al. 1998; La Bella et al. 2002; Smith et al. 2003; Van de Wiele et al. 2001). Consequently, most labeled bombesin analogs are simply modifications of this bombesin-(7–14) sequence (Baidoo et al. 1998; La Bella et al. 2002; Smith et al. 2003; Van de Wiele et al. 2001; Van de Wiele et al. 2000). In this case, modification of the bombesin-(7–14) peptide was carried out to include a second $\beta$-alanine extension in position six, replacing the non-essential D-Tyr (Fig. 1). This was completed to ensure that the active region of the ligand is situated away from the nanoparticle core.

An N-terminal alkyne substituent has also been installed to allow for a highly chemoselective and functional group tolerant Cu(I) catalyzed "click" cycloaddition reaction with an azide on the SPIO surface to be carried out. This cycloaddition reaction can be carried out in aqueous conditions, and has been found to be very high yielding, even in the presence of significant steric hindrance (Kolb and Sharpless 2003; Lutz and Zarafshani 2008). It has previously been demonstrated to be effective for conjugating molecules to the surface of SPIO (Martin et al. 2008; Sun et al. 2006; White et al. 2006), and is particularly promising for biomacromolecules such as peptides, as the alkyne functionality is orthogonal to all other functionalities occurring in natural amino acids. In contrast to traditional peptide conjugation strategies which involve functionalities such as thiols (Josephson et al. 1999; Montet et al. 2006) or carboxylic acids (Reynolds et al. 2005) on the peptide, it negates the requirement of introducing amino acids such as cysteine into the native peptide solely for conjugation and also overcomes selectivity problems that can be encountered when thiols, carboxylic acids, or amines are required in the peptide for activity.

The target pan-bombesin peptide **1** was synthesized using standard Fmoc solid phase peptide chemistry on an insoluble polystyrene Rink amide 4-methylbenzhydrylamine (MBHA) resin. Through standard coupling methods, propargylacetic acid was attached to the peptide to install the N-terminal alkyne. Typically, only two coupling reactions are required; however, as verified by HPLC, a third overnight coupling was necessary in order for the alkyne attachment to go to completion. The panbombesin peptide was then cleaved from the solid support and purified using preparative HPLC to give 23.5 mg (12% yield) of the desired alkyne product as a white fluffy powder.

### Synthesis of functionalized nanoparticles

Dextran-coated superparamagnetic iron oxide nanoparticles **2** (Scheme 1) functionalized with azides (1 μmol/mg of iron) and the fluorescent rhodamine derivative **3** (0.1 μmol/mg of iron) were prepared as previously reported (Martin et al. 2008; Molday and MacKenzie 1982; Pittet et al. 2006). The absorption maximum of **3** is 560 nm (supporting information), which is outside the tissue penetration window of 650–900 nm (Jobsis 1977), making this chromophore primarily useful for in vitro rather than in vivo studies. However, it is easy to synthesize and manipulate on a large scale, and can easily be substituted in future generations of the agent with a near IR dye such as Cy5.5. This would allow for in vivo

optical imaging. These nanoparticles had an overall hydrodynamic diameter of 15 nm with a small degree of aggregation, resulting in a polydispersity of 0.43 as determined by dynamic light scattering (Fig. 2a). The diameter of the iron oxide core was measured to be 5–10 nm by transmission electron microscopy (TEM) (Fig. 2b). The presence of the azides was verified by infrared (IR) spectroscopy using the distinctive azide stretch at 2,090 cm$^{-1}$ (Fig. 3a). It has been previously demonstrated that the conjugation of the azides to the nanoparticles in this range of loading occurs in high yields (Martin et al. 2008). The quantity of conjugated dye was measured by ultraviolet–visible (UV–vis) spectroscopy to be 0.092 μmol/mg of iron. These nanoparticles were stable for several months at 2–4 °C.

Conjugation of the peptide **1** to nanoparticle **2** was carried out using standard "click" cycloaddition conditions consisting of 2.5 mM CuSO$_4$ and 6.6 mM sodium ascorbate for 24 h in water/DMF (2/1) (Scheme 1). The resulting nanoparticles were purified by dialysis against 10 mM ethylenediaminetetraacetic acid (EDTA), followed by water. The EDTA dialysis was found to be important for the removal of copper which is highly toxic to cells. Following the dialysis, a portion of the sample was lyophilized and analyzed by IR spectroscopy. As shown in Fig. 3b, a significant reduction in the intensity of the azide peak at 2,090 cm$^{-1}$ was observed. However, unlike previous click conjugations carried out with alkyne-functionalized dendrons on iron oxide (Martin et al. 2008), a small peak remained, indicating that the reaction did not reach completion. A number of different reaction conditions such as varying solvents and the use of high pressure were investigated, but it was not possible to reach 100% yield.

Nevertheless, it was important to obtain an approximate quantification of the reaction yield in order to determine the loading of the peptide on the nanoparticles. This was done using semi-quantitative IR spectroscopy. Samples of nanoparticles **2** and **4**, containing equal amounts of iron were lyophilized and each was combined with an equal amount of KBr to prepare a KBr pellet. By comparing the integration of the peak corresponding to the azide stretch prior to (Fig. 3a) and after (Fig. 3b) the conjugation reaction, it was determined that the reaction was approximately 83% complete. A comparison of the integration of the azide peak with the peak at 850 cm$^{-1}$ where there is no contribution from the peptide (Fig. 3c), provided a very similar yield of 80%. As the initial loading of azides on the nanoparticles was very close to 1 μmol/mg of iron, the resulting loading of peptide **1** was approximately 0.8 μmol/mg of iron. Based on a magnetite density of 5.15 g/cm$^3$ and an average core diameter of 7 nm, this corresponds to approximately 300 peptide molecules per nanoparticle.

### Binding and internalization assays

GRP receptors are over-expressed on a variety of human cancer cells including prostate, breast, lung, and pancreatic. The human prostate cancer cell line, PC-3, has been shown to express high levels of GRP receptors (Rogers et al. 2003), so this cell line was used to evaluate the specificity of our GRP receptor-targeted nanoparticles. Nanoparticles **2** and **4**, incorporating the red fluorescent rhodamine dye, were incubated with GFP expressing PC-3 cells and were evaluated by multi-channel fluorescence microscopy. Representative images are depicted in Fig. 4. To quantitate only the intracellular fluorescence, the expression of cytoplasmic GFP was used to constrain the area of measurement. After 2 h of incubation,

significant accumulation of fluorescence signal was observed in the cytoplasm of targeted PC-3 cells incubated with nanoparticle **4**, nearly 300% than that seen with control nanoparticle **2**. Five fields with a minimum of 10 fields per group were analysed, and the experiment was performed in triplicate. The difference was statistically significant ($P$<0.0001). High resolution confocal imaging suggested that internalized nanoparticles localized to the late endosomal/lysosomal compartment, as would be expected following receptor-mediated uptake (Serada et al. 2007). In addition, the nanoparticles co-localized with viral nanoparticles that have been previously demonstrated to localize to the late endosomal compartment (data not shown) (Lewis et al. 2006). Blocking the receptor binding sites with a ten-fold excess of free unlabeled peptide decreased the internalization of nanoparticle **4** to the level of the control nanoparticle **2**. This demonstrates the specificity of the peptide-labeled nanoparticles for bombesin receptors expressed on PC-3 cells and further indicates that this imaging probe does in fact undergo internalization upon receptor binding.

While the zeta potentials of the nanoparticles was not explicitly measured, the surfaces of both nanoparticles **2** and **4** should to be cationic due to the amine-modified dextran coating (Pittet et al. 2006) and the neutral charge of the conjugated peptides. As cationic iron oxide nanoparticles have been found to be taken up by cells much more effectively than their anionic counterparts (Song et al. 2005; Montet et al. 2006), this may lead to some of the nonspecific uptake of nanoparticle **2** by the PC-3 cells. This suggests that even greater targeting specificity may be achieved by the conjugation of peptide **1** to neutral or anionic nanoparticles.

## Conclusions

In conclusion, an alkyne-functionalized analog of bombesin was prepared and conjugated to dye-functionalized dextran-coated superparamagnetic iron oxide nanoparticles. Click cycloaddition conditions were used for the conjugation, and these conditions provided a complementary approach to traditional peptide conjugation conditions. The yield for this conjugation was found to be approximately 80%, which was determined by IR spectroscopy, providing the advantage that it was not necessary to functionalize the peptide with a dye molecule prior to its conjugation solely for quantification. Using the fluorescence of the dye molecules on the nanoparticles for confocal fluorescence microscopy experiments, it was found that nanoparticle **4** was selectively taken up by PC-3 cancer cells in vitro relative to unfunctionalized nanoparticle **2**. Experiments performed in the presence of excess free peptide confirmed that the uptake was indeed due to the peptide. Thus, this nanoparticle system represents a potential new imaging probe, and demonstrates for the first time that bombesin is a highly promising targeting ligand for delivering not only small molecule radioisotopes but also nanoparticles into prostate cancer cells. Thus, these targeted nanoparticles may be useful for the diagnosis of prostate cancer and can also potentially serve as a platform for the delivery of drug molecules. Future work will involve an investigation of the effect of surface charge on cell uptake, the replacement of the fluorescent rhodamine with a near-IR dye, and a study of the biodistribution behavior in vivo using optical and MR imaging.

## Supplementary Material

Refer to Web version on PubMed Central for supplementary material.

## Acknowledgments

## References

Alonzi R, Padhani AR, Allen C. Dynamic contrast enhanced MRI in prostate cancer. Eur J Radiol. 2007; 63:335– 350. [PubMed: 17689907]

American Cancer Society. Cancer facts and figures 2007. American Cancer Society; Atlanta: 2007. p. 54

Ametamey SM, Honer M, Schubiger PA. Molecular imaging with PET. Chem Rev. 2008; 108:1501– 1516. [PubMed: 18426240]

Baidoo KE, Lin KS, Zhan Y, Finley P, Scheffel U, Wagner HN Jr. Design, synthesis, and initial evaluation of high-affinity technetium bombesin analogues. Bioconjug Chem. 1998; 9:218–225. [PubMed: 9548537]

Basilion JP, Yeon S, Botnar R. Magnetic resonance imaging: utility as a molecular imaging modality. Curr Top Dev Biol. 2005; 70:1–33. [PubMed: 16338335]

Broccardo M, Falconieri Erspamer G, Melchiorri P, Negri L. Relative potency of bombesin-like peptides. Br J Pharmacol. 1975; 5:221–227.

Cai W, Chen X. Multimodality molecular imaging of tumor angiogenesis. J Nucl Med. 2008; 49:113S– 128S. [PubMed: 18523069]

Caravan P, Ellison JJ, McMurry TJ, Lauffer RB. Gadolinium (III) chelates as MRI contrast agents: structure, dynamics, and applications. Chem Rev. 1999; 99:2293–2352. [PubMed: 11749483]

Chodak GW, Keller P, Schoenberg HW. Assessment of screening for prostate cancer using the digital rectal exam. J Urol. 1989; 141:1136–1138. [PubMed: 2709500]

Girard F, Bachelard H, St-Pierre S, Rioux F. The contractile effect of bombesin, gastrin releasing peptide and various fragments in the rat stomach strip. Eur Pharmacol. 1984; 102:489–497.

Heijmink SW, Futterer JJ, Hambrock T, Takahashi S, Scheenen TWJ, Huisman HJ, Hulsbergen-Van de Kaa CA, Knipscheer BC, Kiemeney LAL, Witjes JA, Barentsz JO. Prostate cancer: Body-array versus endorectal coil MR imaging at 3 T—comparison of image quality, localization, and staging performance. Radiology. 2007; 244:184–195. [PubMed: 17495178]

Hoffman TJ, Gali H, Smith CJ, Sieckman GL, Hayes DL, Owen NK, Volkert WA. Novel series of 111In-labeled bombesin analogs as potential radiopharmaceuticals for specific targeting of gastrin-releasing peptide receptors expressed on human prostate cancer cells. J Nuc Med. 2003; 44:823–831.

Hosseinkhani H, Hosseinkhani M. Biodegradable polymer- metal complexes for gene and drug delivery. Curr Drug Safety. 2009; 4:79–83.

Huzjan R, Sala E, Hricak H. Magnetic resonance imaging and magnetic resonance spectroscopic imaging of prostate cancer. Nat Clin Prac Urol. 2005; 2:434–442.

Ikonen S, Karkkainen P, Kivisaari L, Salo JO, Taari K, Vehmas T, Tervahartiala P, Rannikko S. Endorectal magnetic resonance imaging of prostatic cancer: Comparison between fat-suppressed T2-weighted fast spin echo and three-dimensional dual-echo, steady-state sequences. Eur Radiol. 2001; 11:236–241. [PubMed: 11218020]

Jobsis FF. Noninvasive, infrared monitoring of cerebral and myocardial oxygen sufficiency and circulatory parameters. Science. 1977; 198:1264–1267. [PubMed: 929199]

Josephson L, Tung C, Moore A, Weissleder R. High-efficiency intracellular magnetic labeling with novel superparamagnetic- Tat peptide conjugates. Bioconjug Chem. 1999; 10:186–191. [PubMed: 10077466]

Jun Y, Lee J, Cheon J. Chemical design of nanoparticle probes for high-performance magnetic resonance imaging. Angew Chem Int Ed Engl. 2008; 47:5122–5135. [PubMed: 18574805]

Kelly KA, Setlur S, Ross R, Anbazhagan R, Waterman P, Rubin MA, Weissleder R. Detection of early prostate cancer using a hepsin-targeted imaging agent. Cancer Res. 2008; 68:2286–2291. [PubMed: 18381435]

Kirkham AP, Emberton M, Allen C. How good is MRI at detecting and characterising cancer within the prostate? Eur Urol. 2006; 50:1163–1174. [PubMed: 16842903]

Kolb HC, Sharpless KB. The growing impact of click chemistry on drug discovery. Drug Disc Today. 2003; 8:1128– 1137.

La Bella R, Garcia-Garayoa E, Bahler M, Blauenstein P, Schibli R, Conrath P, Tourwe D, Schibiger PA. A 99mTc(I)-postlabeled high affinity bombesin analogue as a potential tumor imaging agent. Bioconjug Chem. 2002; 13:599–604. [PubMed: 12009951]

Laurent S, Forge D, Port M, Roch A, Robic C, Vander Elst L, Muller RN. Magnetic iron oxide nanoparticles: synthesis, stabilization, vectorization, physicochemical characterizations, and biological applications. Chem Rev. 2008; 108:2064–2110. [PubMed: 18543879]

Lewis JD, Destito G, Zijlstra A, Gonzalez MJ, Quigley JP, Manchester M, Stuhlmann H. Viral nanoparticles as tools for intravital vascular imaging. Nat Med. 2006; 12:354–360. [PubMed: 16501571]

Lutz J, Zarafshani Z. Efficient construction of therapeutics, bioconjugates, biomaterials and bioactive surfaces using azide-alkyne "click" chemistry. Adv Drug Deliv Rev. 2008; 60:958–970. [PubMed: 18406491]

Mantey SA, Weber HC, Sainz E, Akeson M, Ryan RR, Pradhan TK, Searles RP, Spindel ER, Battey JF, Coy DH, Jensen RT. Discovery of a high affinity radioligand for the human orphan receptor, bombesin receptor subtype 3, which deomonstrates that it has a unique pharmacology compared with other mammalian bombesin receptors. J Biol Chem. 1997; 272:26062–26071. [PubMed: 9325344]

Martin AL, Bernas L, Foster PF, Rutt BK, Gillies ER. Enhanced cell uptake of superparamagnetic iron oxide nanoparticles functionalized with dendritic guanidines. Bioconjug Chem. 2008; 19:2375–2384. [PubMed: 19053308]

Molday RS, MacKenzie D. Immunospecific ferromagnetic iron-dextran reagents for the labeling and magnetic separation of cells. J Immunol Methods. 1982; 52:353–367. [PubMed: 7130710]

Montet X, Weissleder R, Josephson L. Imaging pancreatic cancer with a peptide-nanoparticle conjugate targeted to normal pancreas. Bioconjug Chem. 2006; 17:905–911. [PubMed: 16848396]

Nam RK, Toi A, Klotz LH, Trachtenberg J, Jewett MAS, Appu S, Loblaw AD, Sugar L, Narod SA, Kattan MW. Assessing individual risk for prostate cancer. J Clin Oncol. 2007; 25:3582–3588. [PubMed: 17704405]

Padhani AR, Gapinski CJ, Macvicar DA, Parker GJ, Suckling J, Revell PB, Leach MO, Dearnaley DP, Husband JE. Dynamic contrast enhanced MRI of prostate cancer: correlation with morphology and tumour stage, histological grade and PSA. Clin Radiol. 2000; 55:99–109. [PubMed: 10657154]

Patel O, Shulkes A, Baldwin GS. Gastrin releasing peptide and cancer. Biochim Biophys Acta. 2006; 1766:23–41. [PubMed: 16490321]

Pittet MJ, Swirski PK, Reynolds F, Josephson L, Weissleder R. Labeling of immune cells for in vivo imaging using magnetofluorescent nanoparticles. Nat Protoc. 2006; 1:73– 78. [PubMed: 17406214]

Pradhan TK, Katsuno T, Taylor JE, Kim SH, Ryan RR, Mantey SA, Donohue PJ, Weber HC, Sainz E, Battey JF, Coy DH, Jensen RT. Identification of a unique ligand which has high affinity for all four bombesin receptor subtypes. Eur J Pharm. 1998; 343:275–287.

Reubi JC, Wenger S, Schmuckli-Maurer J, Schaer JC, Gigger M. Bombesin receptor subtypes in human cancers: Detection with the universal radioligand I-125-[D-TYR6, beta-ALA(11), PHE13, NLE14] bombesin(6-14). Clin Cancer Res. 2002; 8:1139–1146. [PubMed: 11948125]

Reynolds F, Weissleder R, Josephson L. Protamine as an efficient membrane-translocating peptide. Bioconjug Chem. 2005; 16:1240–1245. [PubMed: 16173804]

Rogers BE, Bigott HM, McCarthy DW, Della Manna D, Kim J, Sharp TL, Welch MJ. MicroPET imaging of a gastrin-releasing peptide receptor-positive tumor in a mouse model of human prostate cancer using a 64Cu-labeled bombesin analogue. Bioconjug Chem. 2003; 14:756–763. [PubMed: 12862428]

Serada RE, Adolphi NL, Bisoffi M, Sillerud LO. Targeting and cellular trafficking of magnetic nanoparticles for prostate cancer imaging. Mol Imaging. 2007; 6:277–288. [PubMed: 17711783]

Smith CJ, Sieckman GL, Owen NK, Hayes DL, Mazuru DG, Kannan R, Volkert WA, Hoffman TJ. Radio-chemical investigations of gastrin-releasing peptide receptor-specific [99mTc(X)(CO)3-Dpr-Ser-Ser-Ser-Gln-Trp-Ala-Val-Gly-His-Leu-Met-NH2] in PC-3, tumor-bearing rodent models; syntheses, radiolabeling, and in vitro/in vivo studies where Dpr = 2, 3-diaminopropionic acid and $X = H_2O$ or $P(CH_2OH)_3$. Cancer Res. 2003; 63:4082– 4088. [PubMed: 12874010]

Song HT, Choi JS, Huh YM, Kim S, Jun YW, Suh JS, Cheon J. Surface modulation of magnetic nanocrystals in the development of highly efficient magnetic resonance probes for intracellular labeling. J Am Chem Soc. 2005; 127:9992–9993. [PubMed: 16011350]

Sun B, Schally AV, Halmos G. The presence of receptors for bombesin/GRP and mRNA for three receptor subtypes in human ovarian epithelial Cancers. Regul Pept. 2000; 90:77–84. [PubMed: 10828496]

Sun EY, Josephson L, Weissleder R. "Clickable" nanoparticles for targeted imaging. Mol Imaging. 2006; 5:122– 128. [PubMed: 16954026]

Tanimoto A, Nakashima J, Kohno H, Shinmoto H, Kuribayashi S. Prostate cancer screening: The clinical value of diffusion-weighted imaging and dynamic MR imaging in combination with T2-weighted imaging. J Magn Reson Imaging. 2007; 25:146–152. [PubMed: 17139633]

Van de Wiele C, Dumont F, Vanden Broecke R, Oosterlinck W, Cocquyt V, Serreyn R, Peers S, Thronback J, Slegers G, Dierckx RA. Technetium-99m RP527, a GRP analogue for visualization of GRP receptor-expressing malignancies: a feasibility study. Eur J Nuc Med. 2000; 27:1694–1699.

Van de Wiele CV, Dumont F, Dierckx RA, Peers SH, Thornback JR, Slegers G. Biodistribution and dosimetry of 99mTc-RP527, a gastrin-releasing peptide (GRP) agonist for the visualization of GRP receptor-expressing malignancies. J Nucl Med. 2001; 42:1722–1727. [PubMed: 11696645]

Wang AZ, Bagalkot V, Vasilliou CC, Gu F, Alexis F, Zhang L, Shaikh M, Yuet K, Cima MJ, Langer R, Kantoff PW, Bander NH, Jon S, Farokhzad OC. Superparamagnetic iron oxide nanoparticle-aptamer bioconjugates for combined prostate cancer imaging and therapy. Chem Med Chem. 2008; 3:1131–1315.

Weissleder R, Pittet MJ. Imaging in the era of molecular oncology. Nature. 2008; 452:580–589. [PubMed: 18385732]

White MA, Johnson JA, Koberstein JT, Turro NJ. Toward the syntheses of universal ligands for metal oxide surfaces: controlling surface functionality through click chemistry. J Am Chem Soc. 2006; 128:11356–11357. [PubMed: 16939250]

Willmann JK, van Bruggen N, Dinkelborg LM, Gambhir SS. Molecular imaging in drug development. Nat Rev Drug Discov. 2008; 7:591–607. [PubMed: 18591980]

Zapotoczna A, Sasso G, Simpson J, Roach M. Current role and future perspectives of magnetic resonance spectroscopy in radiation oncology for prostate cancer. Neoplasia. 2007; 9:455–463. [PubMed: 17603627]

**Fig. 1.**
Chemical structure of an alkyne functionalized pan-bombesin peptide (**1**) for conjugation to SPIO
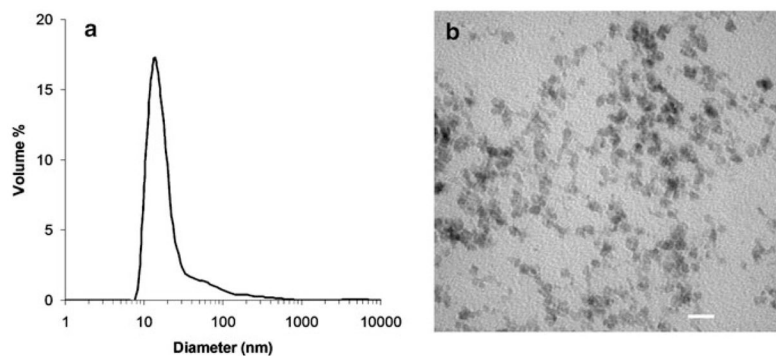
**Fig. 2.**
**a** Size distribution of nanoparticle **2** as determined by dynamic light scattering; **b** Iron oxide cores of nanoparticle **2** as visualized by transmission electron microscopy (scale bar = 20 nm)
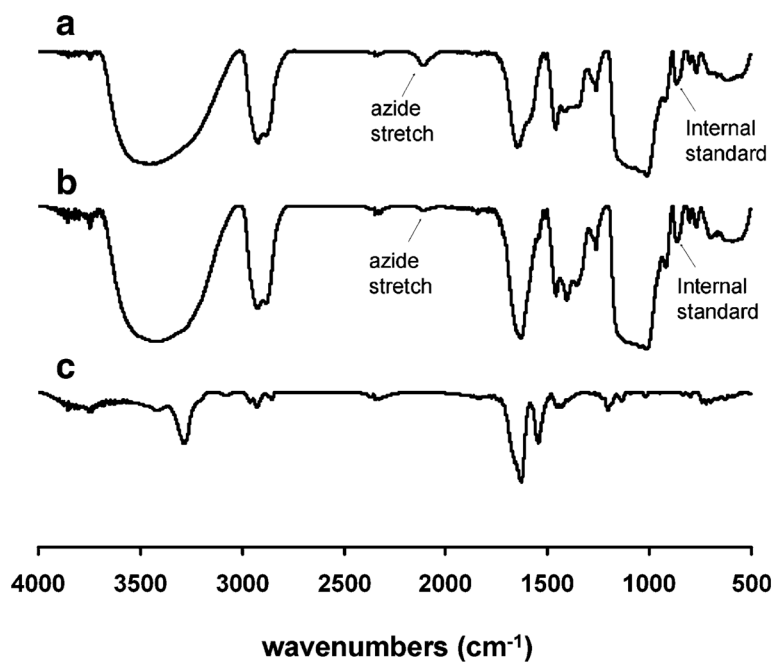
**Fig. 3.**
IR spectra of **a** nanoparticle **2** having a distinctive azide stretch at 2090 cm$^{-1}$, **b** nanoparticle **4** following conjugation of the peptide, showing near disappearance of the azide stretch at 2090 cm$^{-1}$ and **c** peptide **1**
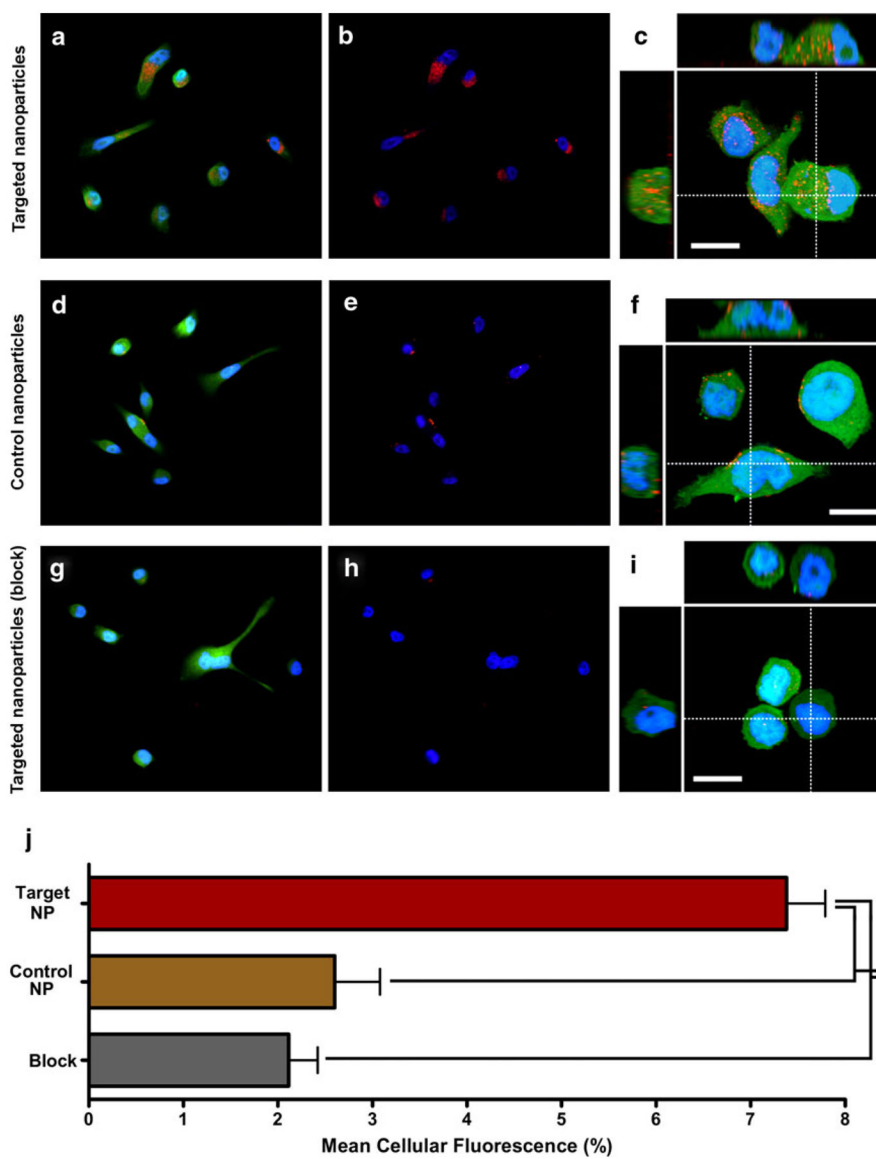
**Fig. 4.**
Binding and internalization of targeted nanoparticles to human prostate cancer cells. **a**, **d**, **g** Visualization of uptake of targeted and control nanoparticles using three-channel fluorescence imaging of adhered PC-3 cells with nuclei (*blue*), cytoplasm (*green*) and nanoparticles (*red*). **b**, **e**, **h** Two-channel fluorescence imaging of adhered PC-3 cells with nuclei (*blue*) and nanoparticles (*red*) using the same fields as **a**, **d**, **g**, **c**, **f**, **i**. High resolution confocal imaging of nanoparticle localization within PC-3 cells with nuclei (*blue*), cytoplasm (*green*) and nanoparticles (*red*). Also shown are XZ (*top*) and YZ (*left*) volume slices corresponding to dotted line. Scale bar is 13 μm. **j** Quantitation of binding and uptake of nanoparticles in prostate cancer cells. Using Volocity software (Improvision, UK), ROIs corresponding to the cancer cell bodies were selected automatically using green channel fluorescence (SD intensity filter). Mean fluorescence of each ROI was then calculated in the red channel corresponding to the nanoparticles using the 14 bit acquired data. Five fields

including a minimum of 10 cells each were analysed and represented in the bar graph as mean cellular fluorescence expressed as a percentage of maximum. Each analysis was performed in triplicate. Statistical significance was determined by one-way ANOVA ($P<0.0001$) (Color figure online)
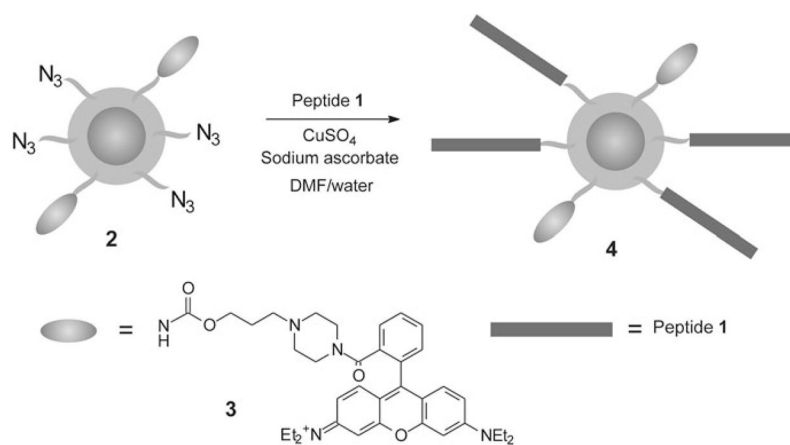
**Scheme 1.**
Synthesis of functionalized nanoparticles